# Different models of the active cochlea, and how to implement them in the state-space formalism

Renata Sisto
*Dipartimento Igiene del Lavoro, ISPESL, Via Fontana Candida 1, 00040 Monte Porzio Catone, Rome, Italy*

Arturo Moleti,[a] Nicolo Paternoster, and Teresa Botti
*Dipartimento di Fisica, Università di Roma "Tor Vergata," Via della Ricerca Scientifica 1, 00133 Rome, Italy*

Daniele Bertaccini
*Dipartimento di Matematica, Università di Roma "Tor Vergata," Via della Ricerca Scientifica 1, 00133 Rome, Italy*

(Received 16 March 2010; revised 18 June 2010; accepted 21 June 2010)

The state-space formalism [Elliott S. J., *et al.* (2007). J. Acoust. Soc. Am. **122**, 2759–2771] allows one to discretize cochlear models in a straightforward matrix form and to modify the main physical properties of the cochlear model by changing the position and functional form of a few matrix elements. Feed-forward and feed-backward properties can be obtained by simply introducing off-diagonal terms in the matrixes expressing the coupling between the dynamical variables and the additional active pressure on the basilar membrane. Some theoretical issues related to different cochlear modeling choices, their implementation in a state-space scheme, and their physical consequences on the cochlear phenomenology, as predicted by numerical simulations, are discussed. Different schematizations of the active term describing the behavior of the outer hair cell's feedback mechanism, including nonlinear and nonlocal dependences on either pressure or basilar membrane displacement, are also discussed, showing their effect on some measurable cochlear properties.
 [DOI: 10.1121/1.3466846]

PACS number(s): 43.64.Kc, 43.64.Jb [BLM] Pages: 1191–1202

## I. INTRODUCTION

Cochlear modeling is a very useful tool for understanding basic cochlear physiology, helping the researcher in the theoretical interpretation of experimental data. It also provides a necessary support for design and optimization of new diagnostic techniques of cochlear function. A cochlear model can be used to run "numerical experiments," in which some sort of stimulus is fed as an input to the model, and the output response is computed. The results of these numerical experiments can be compared with those of analog real experiments, with a twofold purpose. In a first stage, such comparisons help refining and validating the model. In a second stage, a validated model can be used to predict the cochlear behavior in different scenarios, which can also be outside the accessibility range of experimental techniques. A model capable of providing reliable predictions outside the range over which it has been directly tested must be built upon solid ground, i.e., it must be based on a coherent theoretical schematization of the cochlear function, and use a limited number of free parameters.

Linear models can be effectively solved in the frequency domain, either using analytical approximations or numerically, with low computational costs. The same advantage applies to those weakly nonlinear models in which the nonlinearity can be treated as a small perturbation. Unfortunately, nonlinearity is a key feature of the cochlear physiology, strictly related to the quality of hearing, which cannot be considered a small perturbation, except, perhaps, at very low sound levels, close to the auditory threshold. Therefore, researchers interested in the design of hearing aids or cochlear implants, as well as those interested in developing new diagnostics of hearing function, cannot fully rely on the predictions and schematizations of linear or quasi-linear models. Nonlinear models should be solved in the time-domain, with typically high computational costs, which can be effectively decreased using advanced numerical techniques.

Several cochlear models have been discussed and tested in the literature, which include active terms, either linear (Neely and Kim, 1986) or nonlinear (e.g., Talmadge *et al.*, 1998; Lim and Steele, 2002; Moleti *et al.*, 2009), to schematize the active feedback mechanism.

In this study, we use a very convenient state-space formulation (Elliott *et al.*, 2007, Moleti *et al.*, 2009) and *ad-hoc* developed fast and reliable numerical techniques (Bertaccini and Fanelli, 2009; Moleti *et al.*, 2009), to discuss the physical meaning of different cochlear modeling choices, how to implement them in a state-space matrix formalism, and their effect on some basic aspects of the cochlear phenomenology, namely the basilar membrane (BM) response and its nonlinear dependence on the stimulus level. In forthcoming studies, we will focus mainly on other issues, namely the propagation of backward waves along the BM and the otoacoustic emission phenomenology, introducing therefore cochlear roughness as an additional parameter.

[a]Author to whom correspondence should be addressed. Electronic mail: moleti@roma2.infn.it

## II. MODELING ISSUES

### A. Baseline transmission line passive cochlear model

We study here a class of models known as transmission-line models (Furst and Lapid, 1988; Talmadge *et al.*, 1998; Shera *et al.*, 2005), in which the differential pressure $p$ across the BM and the transverse BM velocity $\dot{\xi}$ act as the voltage $V$ and the current $I$ in an analog electrical transmission line.

As in Moleti *et al.* (2009), we refer, as a first approximation, to a simple passive 1-d transmission line cochlear model described by the equations:

$$\frac{\partial^2 p(x,0,t)}{\partial x^2} = \frac{2\rho}{H}\ddot{\xi}(x,t), \tag{1}$$

$$\ddot{\xi}(x,t) + \gamma_{bm}(x)\dot{\xi}(x,t) + \omega_{bm}^2(x)\xi(x,t) = \frac{p(x,0,t)}{\sigma_{bm}}, \tag{2}$$

where $\rho$ is the fluid density, $\sigma_{bm}$ is the BM surface density and $\xi$ the BM transverse displacement at the longitudinal position $x$ and time $t$. We assume a cochlear duct of rectangular constant cross section of constant half-height $H$ and length $L$. Equation (1) is obtained, as usual, assuming the fluid incompressibility, using the boundary condition on the BM:

$$\left.\frac{\partial p(x,z,t)}{\partial z}\right|_{z=0} = 2\rho\ddot{\xi}(x,t), \tag{3}$$

and that on the rigid upper wall:

$$\left.\frac{\partial p(x,z,t)}{\partial z}\right|_{z=H} = 0. \tag{4}$$

Equation (2) describes, for each place, the dynamics of a passive oscillator driven by differential pressure only. Active terms, either proportional to $p$ or to $\dot{\xi}$, will be added later to this basic equation.

In a tonotopically resonant cochlea, the relation between longitudinal position $x$, angular frequency and passive damping constant are set by Greenwood (1990) maps, as in Talmadge *et al.* (1998):

$$\omega_{bm}(x) = \omega_0 e^{-k_\omega x} + \omega_1$$

$$\gamma_{bm}(x) = \gamma_0 e^{-k_\gamma x} + \gamma_1. \tag{5}$$

The local passive quality factor is defined as:

$$Q(x) = \frac{\omega_{bm}(x)}{\gamma_{bm}(x)}. \tag{6}$$

In the limit $k_\omega = k_\gamma$, and $\omega_1 = \gamma_1 = 0$, $Q(x) = Q_0 = \omega_0/\gamma_0$ is a constant, and the maps of Eq. (5) do not explicitly break the scale invariance symmetry. If $k_\omega \neq k_\gamma$, we may define a scale-invariance breaking parameter as:

$$\varepsilon = \frac{k_\gamma - k_\omega}{k_\omega}. \tag{7}$$

In the simple case in which $\varepsilon$ is a constant, the quality factor becomes a power law of frequency:

$$Q(\omega) = Q_0\left(\frac{\omega}{\omega_0}\right)^{\varepsilon}. \tag{8}$$

The first of the $N$ elements of the discretized model includes the middle ear and oval window dynamics and the boundary condition:

$$\left.\frac{\partial p}{\partial x}\right|_{x=0} = 2\rho\ddot{\xi}_{ow}, \tag{9}$$

where $\ddot{\xi}_{ow}$ is the acceleration of the stapes. The dynamical equation for this first element is:

$$\ddot{\xi}_{ow}(t) + \gamma_{ow}\dot{\xi}_{ow}(t) + \omega_{ow}^2\xi(t) = \frac{p(0,t) + G_{me}P_{dr}(t)}{\sigma_{ow}}, \tag{10}$$

where according to Eq. (10) of Talmadge *et al.* (1998), $\gamma_{ow}$, $\omega_{ow}$ and $\sigma_{ow}$ are, respectively, the middle ear damping constant, frequency and the effective oval window density, $P_{dr}$ is the calibrated pressure in the ear canal (for a rigid ear drum), and $G_{me}$, is the middle ear mechanical gain of the ossicles. The middle ear is schematized as a broadband filter, whose parameters must be chosen to match the experimental data on the forward transmission gain (Puria, 2003; Voss and Shera, 2004). A maximum transmission around 1000–1500 Hz and rather large bandwidth are required.

The last element of the discretized cochlea is the helicotrema, which can be described either by a simple pressure release boundary condition, as done in this study:

$$p(L,z,t) = 0 \tag{11}$$

or by more accurate dynamics (Ku, 2008), involving friction terms.

### B. The state space formalism

We briefly recall here the elements of the state space formalism. More details can be found in Elliott *et al.* (2007), Ku (2008), and Moleti *et al.* (2009). Using the NxN finite-difference matrix $\mathbf{F}$ defined by Elliott *et al.* (2007), Eqs. (1), (9), and (11) are synthetically written as:

$$\mathbf{F}P(t) = \ddot{\Xi}(t), \tag{12}$$

where

$$\mathbf{F} = \frac{H}{2\rho(\Delta x)^2}\begin{bmatrix} -\frac{\Delta x}{H} & \frac{\Delta x}{H} & & & & & & & 0 \\ 1 & -2 & 1 & 0 & & & & & 0 \\ 0 & 1 & -2 & 1 & & & & & 0 \\ & & & & \cdots & & & & \\ & & & & & 1 & -2 & 1 & 0 \\ & & & & & & 1 & -2 & 1 \\ 0 & & & & & & & 0 & -\frac{2\rho(\Delta x)^2}{H} \end{bmatrix} \tag{13}$$

and $\Delta x = x_i - x_{i-1} = L/(N-1)$. $P(t)$ and $\ddot{\Xi}(t)$ are N-dimensional vectors of the differential pressure and cochlear partition acceleration.

As in Elliott *et al.* (2007), we cast the dynamic variables $(\dot{\xi}_j(x_j,t), \xi_j(x_j,t))$ of the micromechanical elements in a single vector of state variables $U$ of dimension 2N.

Equations (2) and (10) can be written for the whole set of discrete tonotopic oscillators in the form:

$$\dot{U}(t) = \mathbf{A_E} U(t) + \mathbf{B_E}(P(t) + S(t)), \tag{14}$$

where $S(t)$ is a vector whose only non-null element is the first one, which is equal to $G_{me}P_{dr}$.

The matrix $\mathbf{A_E}$ $(2N \times 2N)$ is block diagonal, each block containing the dynamics of the $i$th resonant tonotopic oscillator:

$$\mathbf{A_E} = \begin{bmatrix} \mathbf{A_1} & & \\ & \cdots & \\ & & \mathbf{A_N} \end{bmatrix}$$

(the same rule applies to $\mathbf{B_E}$ and $\mathbf{C_E}$) (15)

with:

$$\mathbf{A_i} \equiv \begin{bmatrix} -\gamma_{bm}(x_i) & -\omega_{bm}^2(x_i) \\ 1 & 0 \end{bmatrix}, \quad \mathbf{B_i} \equiv \begin{bmatrix} \frac{1}{\sigma_{bm}} & 0 \end{bmatrix}^T,$$

$$\text{for } i = 2, \ldots, N-1,$$

$$\mathbf{A_1} \equiv \begin{bmatrix} -\gamma_{ow} & -\omega_{ow}^2 \\ 1 & 0 \end{bmatrix}, \quad \mathbf{B_1} \equiv \begin{bmatrix} \frac{1}{\sigma_{ow}} & 0 \end{bmatrix}^T,$$

$$\mathbf{A_N} \equiv 0, \quad \mathbf{B_N} \equiv 0,$$

$$\mathbf{C_i} \equiv \begin{bmatrix} 1 & 0 \end{bmatrix}. \tag{16}$$

The block diagonal matrix $\mathbf{C_E}$ $(2N \times 2N)$ selects the odd components of the vector to which it is applied, so that:

$$\mathbf{C_E} U(t) = \dot{\Xi}(t)$$

$$\mathbf{C_E} \dot{U}(t) = \ddot{\Xi}(t). \tag{17}$$

It may also be useful to define here another block diagonal matrix $\mathbf{D_E}$ which selects the even components of the state vector $U$, and which will be used later. Its elements are:

$$\mathbf{D_i} \equiv \begin{bmatrix} 0 & \sigma_{bm}\gamma_{bm}(x_i) \end{bmatrix}. \tag{18}$$

The overall state space equation including boundary conditions can be written in the form:

$$\mathbf{M_{lin}} \dot{U}(t) = \mathbf{A_E} U(t) + \mathbf{B_E} S(t), \tag{19}$$

where $\mathbf{M_{lin}}$ is the $2N \times 2N$ mass matrix of the system:

$$\mathbf{M_{lin}} = \mathbf{I} - \mathbf{B_E}\mathbf{F}^{-1}\mathbf{C_E}. \tag{20}$$

### C. Schematizations of the active mechanism

In transmission line models, active terms can be introduced to simulate the behavior of the active feedback mechanism mediated by the outer hair cells (OHCs). An additional pressure on the BM is explicitly introduced into Eq. (2), which describes its local mechanical properties. The OHC mechanism produces indeed an additional pressure on the BM. As this mechanism is locally activated by the passage of the traveling wave (TW), the pressure is assumed to be proportional either to one or the other of the two dynamical quantities describing the cochlear dynamics, $p$, the fluid pressure on the BM, and $\dot{\xi}$, the BM transverse velocity. If the additional pressure is proportional to the BM velocity, it may be considered as due to a sort of negative resistance, or anti-damping. If the additional pressure is proportional to the local pressure on the BM the effect is similar, in some limited sense, to anti-damping, because the response amplitude is proportional, in the linear limit, to the ratio between the total pressure and the damping constant. Coherently increasing the pressure increases the gain as reducing the damping constant, when nonlinearity plays a minor role. Important differences arise at increasing the stimulus level, as nonlinearity and nonlocality come into action. This will be discussed later, after having introduced the mathematical schematization of the nonlinearity.

A different kind of active term, the delayed stiffness term, has been proposed by Zweig (1991), and adopted, among others, by Talmadge *et al.* (1998) and by Shera *et al.* (2005). A stiffness term is actually proportional to $\xi$, and not to $\dot{\xi}$, so power could not be released or absorbed if the delay were not fine-tuned to correspond, for each frequency component, to a constant fraction of its period. In Talmadge *et al.* (1998), the delays of the two delayed-stiffness terms are chosen in such a way that they approximately act, respectively, as a damping term and an anti-damping term. The peculiarity of delayed-stiffness is to localize anti-damping in a region that is slightly basal to the resonant place, providing the "tall-and-broad" activity patterns needed to reconcile cochlear model predictions with the experimental behavior of the phase of the BM transfer function. In this study we will not discuss time-delayed stiffness terms, focusing ourselves on the other two above-mentioned schematizations.

#### 1. Feed-forward models

Some authors (Lim and Steele, 2002; Kim and Xin, 2005; Moleti *et al.*, 2009) have used a feed-forward (FF) scheme to describe the OHC feedback mechanism, in which the additional pressure exerted on the BM by the OHCs at the cochlear place $x$ is proportional to the total pressure on the BM at a slightly more basal place $x$-$\delta x$. This assumption, which is based on the mechanical and geometrical properties of the OHCs (Lim and Steele, 2002), may be expressed as:

$$q(x) = \alpha p_{TOT}(x - \delta x) = \alpha(p(x - \delta x) + q(x - \delta x)), \tag{21}$$

where $\alpha$ is some function of the BM displacement or velocity expressing the gain of the OHC feedback mechanism, which in a realistic model should be both nonlinear and nonlocal, and which will be discussed later.

Other authors (de Boer and Nuttall, 2009) proposed instead a FF scheme based on the introduction of additional active impedance terms producing an additional pressure at $x + \delta x$ that is proportional to the BM velocity at $x$. Such terms correspond to explicit anti-damping forces, and are qualitatively different from the term proposed by Lim and Steele (2002), as we will discuss later in this study.

Recently, FF models have gained some consideration because some experimental studies of the phase of the BM vibration at the distortion product frequency have questioned

the existence of a backward TW along the BM (He *et al.*, 2007; de Boer *et al.*, 2008). Although other experimental data (Dong and Olson, 2008; Shera *et al.*, 2007) support (directly or indirectly) the existence of a backward TW, de Boer and Nuttall (2009) have suggested that the so-called inverted direction of wave propagation (IDWP) could be explained by FF models, which tend to selectively amplify the forward waves only.

The FF mechanism is easily implemented in the state space formalism by introducing two matrices coupling $q$ to $p$, whose non-trivial elements are aligned along a minor diagonal:

$$\mathbf{B}Q(t) = \mathbf{C}P(t). \tag{22}$$

$Q(t)$ and $P(t)$ are, respectively, the column vectors for $q(x_i,t)$ and $p(x_i,t)$. The matrix $\mathbf{B}$ has 1's on its diagonal, and off-diagonal nonzero elements:

$$\mathbf{B}(i+K,i) = -\alpha(x_i,\xi,t) \quad \text{for} \quad i = 0,1,\ldots,N-K, \tag{23}$$

where $K$ is a positive integer.

The matrix $\mathbf{C}$ is a matrix whose nonzero elements are:

$$\mathbf{C}(i+K,i) = \alpha(x_i,\xi,t) \quad \text{for} \quad i = 0,1,\ldots,N-K. \tag{24}$$

The model is changed into the corresponding feed-backward model by taking a negative $K$. After same manipulations it can be shown that the following equation for the state vectors $U$ holds:

$$\mathbf{M_{nl}}\dot{U}(t) = \mathbf{A_E}U(t) + \mathbf{B_E}S(t), \tag{25}$$

where the nonlinear mass matrix is:

$$\mathbf{M_{nl}} = (\mathbf{I} - \mathbf{B_E}\mathbf{G}(U)\mathbf{F^{-1}}\mathbf{C_E}) \tag{26}$$

and $\mathbf{G}(U)$ is the N×N gain matrix:

$$\mathbf{G}(U) = \mathbf{B^{-1}}\mathbf{C} + \mathbf{I}. \tag{27}$$

Neglecting the phase mismatch, which becomes important only over a wavelength scale ($\gg$100 $\mu$m, whereas the FF step should be of order 10 microns), the FF mechanism implies a sort of "pile-up" phenomenon, which, in the simplest case, $K=1$, can be roughly described by a geometrical series:

$$\begin{aligned} p_{TOTi} &= p_i + q_i = p_i + \alpha(p_{i-1} + q_{i-1}) \\ &= p_i + \alpha(p_{i-1} + \alpha(p_{i-2} + q_{i-2})) \\ &= p_i + \alpha(p_{i-1} + \alpha(p_{i-2} + \alpha(p_{i-3} + q_{i-3}))) \\ &= \sum_{k=0}^{N} p_{i-k}\alpha^k \approx \langle p\rangle \frac{1-\alpha^N}{1-\alpha} \approx \frac{\langle p\rangle}{1-\alpha}, \end{aligned} \tag{28}$$

where $p$ is the unperturbed pressure on the BM of the underlying passive model. Therefore the active gain associated with a FF mechanism is predicted to be of order $1/1-\alpha$.

This rough estimate may be useful to compare the expected active gain of FF models with that of simpler anti-damping (AD) models, but it is not accurate enough, as shown by numerical simulations in Section III, to describe the actual active gain of a FF model.

#### 2. A "diagonal" variation

One could be interested in evaluating the effect of an additional active force proportional to pressure in a simpler case, that we define "diagonal" because there is no FF shift, and, therefore, no off-diagonal element in the matrices coupling the additional pressure with the fluid or total pressure. To avoid "circular" contradictions, in this "diagonal" model the additional pressure must be proportional to the fluid local pressure and not to the total pressure on the BM (as in the FF model):

$$q_i = \beta p_i. \tag{29}$$

In this case there is no pile-up, and the pressure amplification is simply:

$$p_{TOTi} = p_i(1+\beta). \tag{30}$$

The alternative formulation using an explicit anti-damping term, either FF (de Boer and Nuttall, 2009) or diagonal, can also be easily implemented in the state space formulation, as explained in Moleti *et al.* (2009), using the mass matrix:

$$\mathbf{M'_{nl}} = \mathbf{I} - \mathbf{B_E}\mathbf{F^{-1}}\mathbf{C_E} + \mathbf{B_E}\mathbf{C}\mathbf{D_E}, \tag{31}$$

where the index $K$ in Eq. (24) defining the matrix $\mathbf{C}$, is zero in the diagonal case, and positive for a FF model.

#### 3. Nonlinear damping

Realistic anti-damping terms are also proportional to some nonlinear function of the BM displacement amplitude and/or velocity. The simplest and best-known form of this term is that of the Van der Pol oscillator:

$$\frac{p_{add}}{\sigma_{bm}} = -(a\xi^2 - b)\dot{\xi}, \tag{32}$$

in which the nonlinear function consists of a constant anti-damping term and a quadratic damping term, whose competition fixes the amplitude of limit-cycle oscillations, for an isolated oscillator. Although models based on this oscillator can be capable of predicting spontaneous oscillations and distortion products, the functional form of the Van der Pol oscillator does not provide a realistic schematization of the OHC filter physiology. In the real case, the anti-damping additional force should not increase indefinitely as the BM displacement increases, but it should saturate instead to some constant value at very high displacement amplitudes. Additionally, there should be a linear response range (with constant positive damping parameter) also at low displacement levels, whereas the Van der Pol oscillator is always nonlinear above its limit-cycle level. As regards spontaneous otoacoustic emissions, their explanation in terms of the noise-driven response of limit-cycle oscillators is being discarded in the recent literature, in favor of less local theories involving formation of steady-state oscillations between the base and the resonant place (Shera, 2003). Indeed, the experimental data on the BM response suggest that it is approximately linear both at very low and very high displacement levels, whereas it is compressively nonlinear in an intermediate displacement level range (see e.g., Kanis and de Boer, 1993; Nobili and Mammano, 1996). More refined descriptions of the OHC

physiology may be expressed by different damping and antidamping terms. Such a behavior may be modeled, for example, by introducing an additional force represented by a nonlinear function of the form:

$$F_{add} = \Gamma_{nl}(\xi)\dot{\xi}$$

$$\Gamma_{nl}(\xi) = (\gamma_{bm} - \Gamma_a)\left(1 - \tanh\left(\frac{\xi^2}{\xi_{sat}^2}\right)\right), \tag{33}$$

where $\xi_{sat}$ is the nonlinear damping displacement scale, around which the above-mentioned transition between the two asymptotic linear regimes occurs. In Eq. (19) of Moleti *et al.* (2009) a slightly different function was used, with similar asymptotic behavior. If this additional pressure term is moved to the first term of Eq. (2), the term proportional to the velocity, which we may call the "effective damping function" becomes:

$$\Gamma_{eff}(\xi) = \gamma_{bm} - (\gamma_{bm} - \Gamma_a)\left(1 - \tanh\left(\frac{\xi^2}{\xi_{sat}^2}\right)\right). \tag{34}$$

This effective damping term is approximately constant at low ($\Gamma_{eff}=\Gamma_a$) and high ($\Gamma_{eff}=\gamma_{bm}$) displacement levels, and the damping increases quadratically in the low to intermediate displacement level range, so it may be used to represent the characteristics of the cochlear amplifier in a wide range of levels, by appropriately tuning the few free parameters $\xi_{sat}$, $\Gamma_a$, and $\Gamma_p$.

In Eq. (33) we have put the instantaneous local BM displacement value, for simplicity of notation, but one could argue that, as $\xi$ is an oscillating function, the effective damping constant of Eq. (34) would rapidly decrease at each zero-crossing of the instantaneous local displacement, particularly when $\Gamma_a$ is much smaller than $\gamma_{bm}$. Apart from the numerical problems that would arise from that, we prefer a model in which the effective local damping is sensitive to the some rms value of the BM displacement, because it seems unreasonable that, at each cochlear place for which the displacement is higher than $\xi_{sat}$, the active amplification is continuously switched on and off by the fast oscillations of the BM displacement. In the next subsection, this "averaging" issue will be discussed, introducing a nonlocal dependence.

At low and high stimulus levels the system is linear, therefore its response is simply proportional to the ratio between the pressure and the effective damping constant. Active terms increase this gain either by increasing the pressure at $x$ with respect to that of the corresponding passive model, as in Eq. (28) or in Eq. (30), or by decreasing the effective damping constant, as in Eq. (34). In the following we will provide a description of the active gain that permits to compare different models of the OHC feedback.

In the case of Eq. (34), we can define an "active gain factor" as the ratio between the cochlear gain at a given BM displacement level and the passive gain:

$$g = \frac{\gamma_{bm}}{\Gamma_{eff}(\xi)} = \frac{1}{1 - \frac{\gamma_{bm} - \Gamma_a}{\gamma_{bm}}\left(1 - \tanh\left(\frac{\xi^2}{\xi_{sat}^2}\right)\right)} \tag{35}$$

which, for $\xi \to 0$, is equal to:

$$g_{\max} = \frac{\gamma_{bm}}{\Gamma_a} \tag{36}$$

and approaches unity for $\xi \gg \xi_{sat}$. If the additional pressure is assumed proportional to the total pressure at a more basal place, in a FF scheme, as in Eq. (28), the nonlinear dependence on the BM displacement $\xi$ can be put in the form of the function $\alpha$. For example:

$$\alpha(\xi) = \alpha_0\left(1 - \tanh\left(\frac{\xi^2}{\xi_{sat}^2}\right)\right) \tag{37}$$

corresponds to an additional pressure which is a constant fraction of the fluid pressure at low levels of the BM displacement, and which goes to zero as the BM displacement exceeds the nonlinear saturation value $\xi_{sat}$.

According to Eq. (28), this would imply an active gain factor:

$$g' = \frac{1}{1 - \alpha_0\left(1 - \tanh\left(\frac{\xi^2}{\xi_{sat}^2}\right)\right)} \tag{38}$$

with:

$$g'_{\max} = \frac{1}{1 - \alpha_0}, \tag{39}$$

for $\xi \to 0$, and equal to unity for $\xi \gg \xi_{sat}$.

From Eqs. (34) and (37), we see that $g=g'$ if the constant $\alpha_0$ is set to:

$$\alpha_0 = \frac{\gamma_{bm} - \Gamma_a}{\gamma_{bm}}. \tag{40}$$

This relation permits to translate a FF model with additional pressure proportional to total pressure on the BM into a corresponding diagonal AD model.

In the diagonal model case of Eq. (30), the gain is:

$$g'' = \frac{p_{TOT}}{p_0} = 1 + \beta(\xi). \tag{41}$$

To get the same "universal" gain functional dependence of Eqs. (35) and (38), the function $\beta$ must satisfy the relation:

$$\beta(\xi) = \left(\left(\alpha_0\left(1 - \tanh\left(\frac{\xi^2}{\xi_{sat}^2}\right)\right)\right)^{-1} - 1\right)^{-1}. \tag{42}$$

The behavior of the theoretical gain function is shown in Fig. 1, as a function of the ratio $\xi/\xi_{sat}$. It is important to set this parameter at the right level, to match the experimental dependence of the BM response on stimulus level. As requested by experimental evidence, in Fig. 1 the gain is constant both at low and high BM displacement levels, and the compressive nonlinearity is approximately quadratic, as shown by the slope of the gain factor. It should be remembered that the apparently narrow compressive range of about one decade in terms of $\xi$ would correspond, as in the real case, to about three decades of stimulus level range, assuming a cubic nonlinearity ($\xi \propto p^{1/3}$). Another parameter which is related to this issue is the quality factor of the underlying passive model, which must be rather small, to match the poor

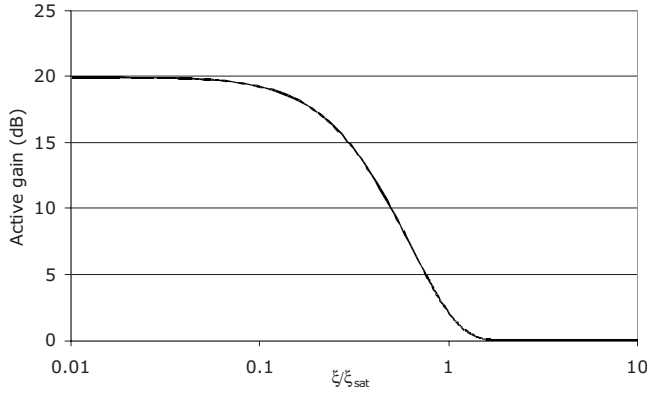


FIG. 1. Theoretical active gain factor for $\alpha_0=0.9$. Two linear damping regions are present at low and high BM displacement levels. In the nonlinear intermediate region, the slope approximately corresponds to that of a quadratic saturation (40 dB/decade). This implies that in this range the response grows approximately as the cubic root of the stimulus. Therefore, the narrow nonlinear range in terms of BM displacement (20 dB) would correspond to a much wider range of stimulus level (≈60 dB), due to saturation itself.

tuning properties of the cadaver cochlea and the strong reduction of the cochlear gain and tuning at high stimulus levels. It is interesting to note that, particularly if the passive quality factor is high, a peculiar phenomenon may occur in the model: the "nonlinear" BM displacement level range is "crossed" too fast by the increasing and oscillating TW response, so the nonlinear range corresponds to the rms BM displacement level at some cochlear place more basal than the resonant place. If the cochlea is driven by two tones of nearby frequencies, $f_1<f_2$, the usual place of origin of the distortion product $(x(f_2))$ would be characterized by quasi-linear response, producing no DP, and the DP source could be shifted to the above-mentioned more basal region. This possibility should be considered when designing a model, and experimental evidence should suggest whether such a phenomenon actually occurs in the real cochlea or it is a fault of the model that should be avoided.

At low levels of the BM displacement, the gain is approximately, in all three cases, using Eq. (39):

$$g = g' = g'' \cong \frac{1}{1-\alpha_0\left(1-\left(\frac{\xi^2}{\xi_{sat}^2}\right)\right)} = \frac{g_{\max}}{\left(1+\frac{\alpha_0}{1-\alpha_0}\left(\frac{\xi^2}{\xi_{sat}^2}\right)\right)}, \tag{43}$$

showing that these models imply quadratically increasing effective damping at low BM displacement levels.

As mentioned above, the approximate equivalence of the "anti-damping" and "additional pressure" models is expected to be broken, considering the distributed nature of the cochlear response (the response to a given frequency is not that of a point-like resonator) and the different role played by the term proportional to BM velocity "close to" and "far from" the resonant place. For each frequency, only close to the resonant place, the left hand side of Eq. (2) is dominated by the term proportional to BM velocity. At high stimulus levels, nonlinearity is important, and the two models predict significantly different responses, also because the cochlear response to a tone of a given frequency cannot be seen as that of a point-like resonator localized in the tonotopic place. The transmission and amplification properties of the BM region basal to the resonant place play a major role and are significantly different in the two cases. In a nonlinear regime, an "additional pressure" active term would selectively increase the cochlear gain in a region more basal than the tonotopic place. In fact, at the resonant place, the BM displacement is maximum and the nonlinear active gain would be correspondingly lower. An active "anti-damping" term would reduce instead the effective damping constant, with little effect far from the resonance, where the term proportional to BM velocity is not dominant in Eq. (2). As a consequence, the "anti-damping" model predicts lower gain and steeper BM response profiles.

### 4. Nonlocality

In a reasonable cochlear model, the dependence of the active gain on the BM displacement level is not expected to be local. Indeed, several psychoacoustic, electrophysiological and otoacoustic experiments have shown that the gain and the bandwidth itself of the cochlear active filter are affected by suppression phenomena within the critical bandwidth. In a more refined cochlear model the active filter gain is therefore some function of the BM displacement level averaged over the cochlear region associated with the critical bandwidth. As a first approximation, a Gaussian average of the BM displacement level over a region of constant width can be used as the variable on which the active gain depends. In Eq. (21) and, equivalently, in Eq. (33), we propose a formulation similar to that proposed by Kim and Xin (2005), with a noteworthy difference:

$$\alpha(x,\xi,t) = \alpha_0\left(1-\tanh\left(\frac{1}{\sqrt{\lambda\pi}}\int_0^L \exp\left(-\frac{(x-x')^2}{\lambda}\right)\times\frac{\xi^2(x',t)}{\xi_{sat}^2}dx'\right)\right), \tag{44}$$

where λ is the square of the length scale of the nonlocal longitudinal interaction range. Here we have chosen to evaluate the active gain function on the Gaussian spatial average of $\xi^2$, instead of taking the average of the same function of the local $\xi^2$. Indeed, $\xi$ is an oscillating function, and any reasonable active gain function is rapidly variable when its argument crosses zero. As a consequence, using the Eq. (19) of Moleti *et al.* (2009), the instantaneous gain would not be sensitive to the "spatial rms" BM displacement, but on the fact that for (at least) one of the discrete spatial elements within $\sqrt{\lambda}$ the solution is very close to zero. A "time rms" average would equally solve this numerical problem, but this solution is preferable, because a spatial average has to be done anyway, and because it is also simpler to be implemented in the numerical solution scheme.

### 5. The semidiscrete model and time step integration

We note that the underlying equations of the models of Eqs. (25), (26), and (31) are *semidiscrete* because the partial derivatives in Eqs. (1)–(4) with respect to the BM displacement are approximated by finite differences, generating a

sequence of systems of $2N$ differential equations parametrized by the space step $\Delta x$ (see Moleti *et al.*, 2009). Moreover, the equations of the semidiscrete model(s) are fully coupled because of the presence in the expression of the mass matrices Eq. (26) and Eq. (31) of the inverses of matrices **F** and **B** defined in Eq. (13) and Eq. (23), respectively. Therefore, in order to avoid an unfeasibly high computational load, both in terms of memory space and number of floating points operations of $O(N^3)$ per time step at least, we propose to implicitly decouple the systems of differential equations of the models Eqs. (25), (26), and (31) and use an implicit time marching scheme similarly to what we have done in Moleti *et al.* (2009).

Let us recall two important issues concerning our approach to the numerical solution of the underlying models. We use here an implicit time step integrator because the numerical solution of a system of differential equations with a nontrivial mass matrix using an explicit time marching scheme requires, at each time step, the solution of a discrete problem (a system of nonlinear algebraic equations), so the computational advantage over a more stable implicit scheme is lost.

In order to advance in time, we require to solve linear systems of the form $\mathbf{A}=\mathbf{M}-h\mathbf{J}$, where, **J** is a constant matrix with few nonzero entries and **M** is the mass matrix that, for the FF model, is given by:

$$\mathbf{M} = \mathbf{I} - \mathbf{B_E}\mathbf{B}^{-1}\mathbf{F}^{-1}\mathbf{C_E}, \tag{45}$$

while, for the "diagonal anti-damping" variation, it is as in Eq. (31). As mentioned above, we need to circumvent inversion of matrices **B** (changing at each step because depending on the BM displacement) and **F** (constant) in Eq. (45).

The key idea is the use of an iterative algebraic linear system solver that at each iteration does not need explicitly forming the matrix **A** and thus **M**, i.e., without performing the matrix inversions at each time step. In view of this, we propose to use a hybrid solver based on a Krylov subspace solver (GMRES). In particular, the Krylov subspace solver approximates the solution of the linear system with matrix **A** requiring the latter only for doing matrix-vector products of the form:

$$w = \mathbf{A}v = \mathbf{M}v - h\mathbf{J}v. \tag{46}$$

Therefore, in order to complete the task in practice, we just need to perform matrix-vector products with matrices $\mathbf{B_E}$, $\mathbf{C_E}$ and to solve two banded linear systems with matrices **B** and **F** for Eq. (45). These strategies are the main building blocks of our customized code based on the Matlab ode15s package.

## III. RESULTS AND DISCUSSION

Numerical simulations have been performed to evaluate the BM response to pure tones of frequency $f_0=2$ kHz, as a function of the stimulus level and of the nonlinear displacement scale, for:

(1) AD: a diagonal model with anti-damping (proportional to BM velocity).
(2) FF: a feed-forward model with additional force proportional to pressure.

Apart from the value of the quality factor of the linear underlying model and of the nonlinear gain parameter $\alpha_0$, explicitly reported for each simulation, the parameters of the model are those reported in Moleti *et al.* (2009). The steady-state BM response has been evaluated as a function of the cochlear position using a total time of 20 ms, amply sufficient to reach steady state in the stable cases (the forward cochlear transmission latency is of order 3–4 ms at 2 kHz), which also permits, when necessary, to get Fourier spectra with 50 Hz resolution. The stimulus is fed to the first element of the model, which represents the middle ear and the oval window, as an additional pressure, converted into an equivalent pressure in the ear canal following Talmadge *et al.* (1998), as done in Moleti *et al.* (2009). Ear canal stimuli in the range 45–110 dB SPL, and nonlinear damping displacement scales $\xi_{sat}$ in the range 1–10 000 nm, which allowed us to fully explore the three different ranges of the nonlinear BM response. When studying the response as a function of the stimulus level, the nonlinear damping displacement scale $\xi_{sat}$ has been set to 100 nm, whereas the stimulus level has been fixed at 80 dB SPL in the simulations at variable $\xi_{sat}$. The cochlear gain has been evaluated as the ratio between the maximum of the Fourier Transform (FT) component at frequency $f_0$ of the BM displacement [which is reached close to the resonant place $x(f_0)$] and the stimulus level. At very high stimulus levels the response is expected to become linear, because the nonlinear terms of Eqs. (32) and (36) become negligible. This asymptotic linear passive gain has been used as a reference for the dB scale used in the figures shown in the next subsections, where the theoretical active gain predicted by Eqs. (34) and (37) is compared with the results of numerical simulations.

In these simulations we used $N=1000$ cochlear partitions and a FF step equal to $K=1$ discrete element. This means that the FF shift is $\delta x=\Delta x=35$ $\mu$m is all simulations. Of course, this is a critical parameter, which should be tuned to best represent the actual geometry of the OHCs. The reasons for choosing this value of $\delta x$ are: 1) it is the minimum shift permitted by $N=1000$ simulations, which are sufficiently fast to be handled, and 2) it is within the same range explored by other modeling studies in the literature (Geisler and Sang, 1995; Lim and Steele, 2002; de Boer and Nuttall, 2009). More detailed studies involving a smaller value of $\delta x$ would obviously require larger values of N and higher computational costs.

### A. BM resonant response

First we show the results of a simulation for a sinusoidal stimulus at $f_0=2$ kHz, in a AD model whose nonlinear term is an additional force proportional to the BM velocity, as in Eq. (33), with $Q=2$, and $\alpha_0=0.9$. In Fig. 2 the computed BM response to a pure tone stimulus of 60 dB SPL in the ear canal is shown in the bottom panel as a function of time at the resonant place $x(f_0)=16$ mm, and at two more basal cochlear positions, $x=9$ mm $x=12.3$ mm, in the top and in the mid panel. The time-domain solution provides the time dependence of the solution at any place, without any as-

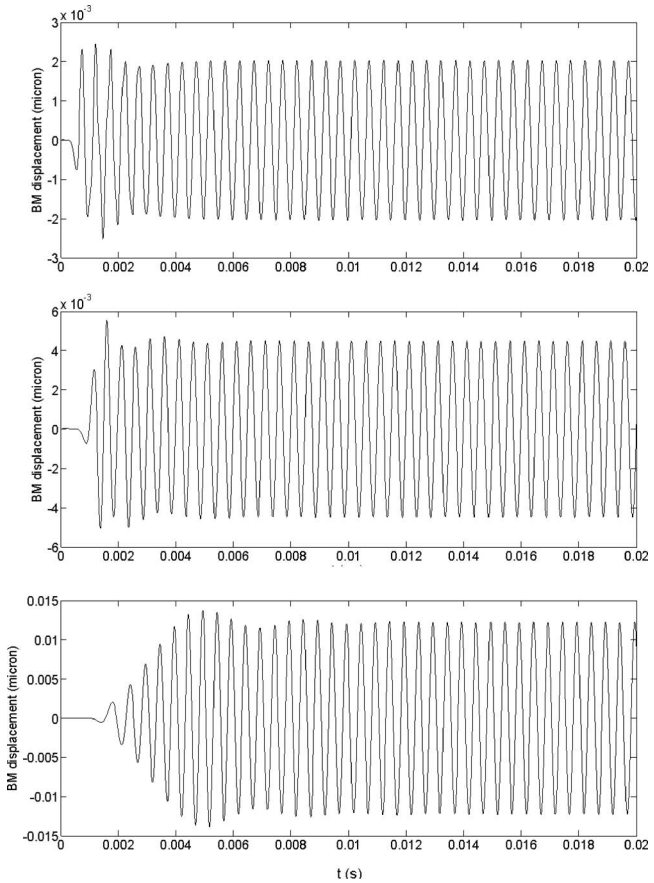


FIG. 2. Computed BM response to a pure tone stimulus of frequency $f_0$ =2 kHz (60 dB SPL in the ear canal), as a function of time at the resonant place $x(f_0)$, and at two more basal intermediate positions. The progressive onset of the response at different cochlear places is visible. The slow envelope overshoot at the onset is the effect of the nonlocal and nonlinear nature of the active mechanism, which implies that the active gain is sensitive to the instantaneous BM displacement level of nearby cochlear regions. These features are effectively studied only using time-domain solutions.

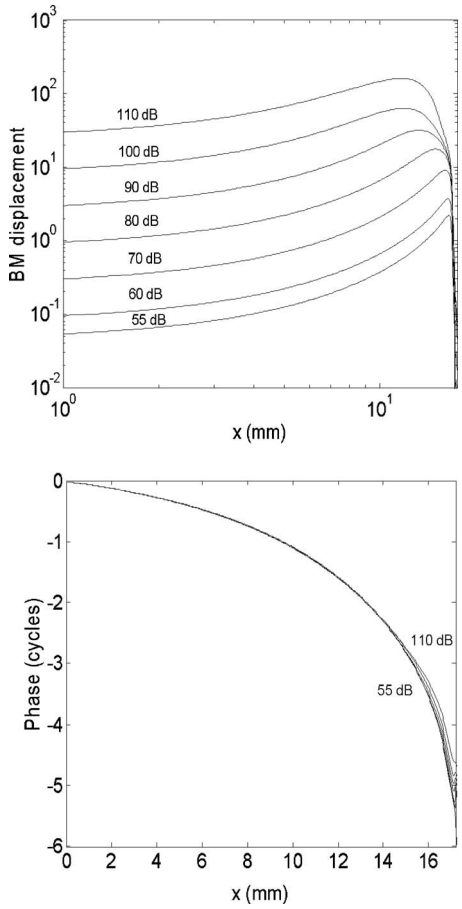


FIG. 3. (Top panel) Amplitude of the Fourier component at frequency $f_0$ of the BM response to a sinusoidal stimulus as a function of the cochlear position $x$, for stimulus levels increasing, from left to right, between 55 and 110 dB. With increasing stimulus level, the gain decreases and the bandwidth increases. (Bottom panel) Corresponding phase, showing that the phase slope (strictly related to forward cochlear latency in a scale-invariant model) close to the resonance decreases with increasing stimulus level.

sumption about the size of the nonlinearity. The onset of the response is clearly visible at increasing delays between 1 and 5 ms.

The Fourier component at frequency $f_0$ (amplitude in a.u., and phase in cycles) of the local response is plotted in Fig. 3 as a function of $x$, showing the expected resonant behavior, for stimulus levels between 55 and 110 dB. With increasing stimulus level, the response grows nonlinearly, the bandwidth increases, the peak position shifts toward the base, and the phase slope decreases. At the highest stimulus levels, linear response is evidently recovered (the response curves become similar to each other and equally spaced), with the low $Q$ value corresponding to the underlying passive model. All these features qualitatively match (with obvious differences associated with the different cochlear size and frequency response) those observed in BM vibration experimental "in vivo" studies on small mammals (e.g., Ren and Nuttall, 2001; Rhode, 2007). In these experiments the observed cochlear position is usually fixed and the frequency is changed, but scale-invariance permits to compare the two "dual" representations. For this reason we have used a logarithmic scale for the cochlear position $x$, to permit a visual comparison with the typical "frequency response" plots usually shown in BM vibration experimental studies.

The numerical solution of the FF model showed significant differences if compared with the theoretically correspondent diagonal AD model. First of all, the apparently "safe" [according to Eq. (28)] choice $\alpha_0$=0.9 leads to a sort of "instability," which means that, if one performs simulations with fixed stimulus level and increasing $\xi_{sat}$, the response saturates around the nonlinear displacement scale, almost independently of how much one decreases the stimulus level. Therefore, to compare the FF model with the diagonal AD model, a lower value of $\alpha_0$ has been used, empirically set to 0.7 to roughly match the stable behavior and the maximum active gain level (20 dB) of the AD model with $\alpha_0$ =0.9. In Fig. 4 we show the BM displacement (amplitude and phase) of the FF model as a function of $x$, for stimulus levels between 50 and 110 dB SPL. Compared with the response of the AD model, the nonlinear growth of the response is still present but it is less evident, the bandwidth is large also at low BM displacement levels (for which the active mechanism is effective), and the basal shift of the resonant peak position at high stimulus levels is less pronounced. The slope of the phase at the resonant place is also less steep than that of the AD model.

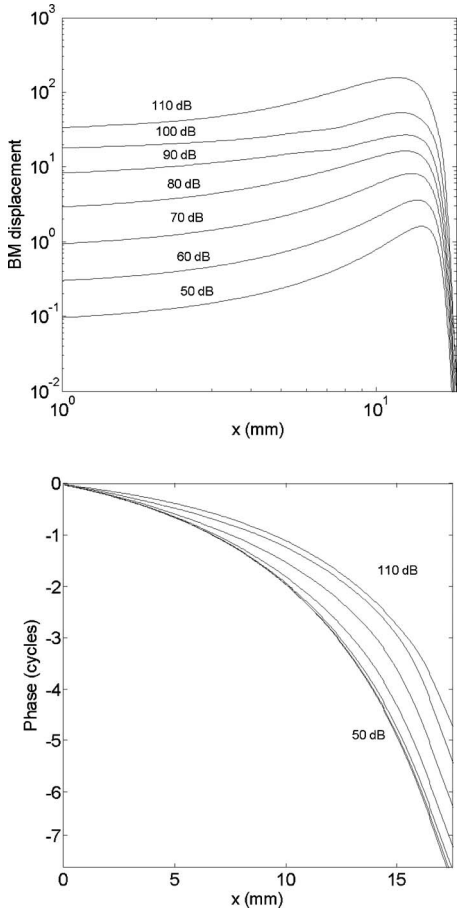


FIG. 4. BM displacement (amplitude and phase) as a function of $x$, for a FF model with Q=2 and $\alpha_0$=0.7, for stimulus levels between 50 and 110 dB SPL.

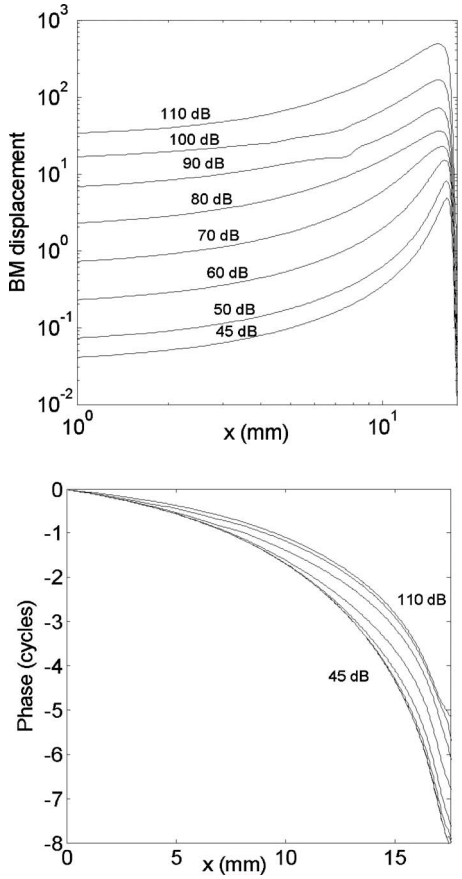


FIG. 5. BM displacement (amplitude and phase) of a FF model with Q=8 and $\alpha_0$=0.6, for stimulus levels between 45 and 110 dB SPL.

To get a more peaked response from a FF model a higher value of passive $Q$ is required. It turned out that the effectiveness of the FF amplifier is also higher for higher values of $Q$, so in Fig. 5 we show the response of a FF model with $Q$=8 and a lower value of $\alpha_0$=0.6, for stimulus levels between 45 and 110 dB SPL. Steep phases and narrow bandwidth resonances are obtained, obviously, comparable with those of the AD model, but some FF characteristics, such as the reduced basal shift of the peak position at high stimulus levels, are still present.

### B. Active gain

The dependence on the stimulus level of the peak response is shown in Fig. 6 for the AD model to allow a visual comparison with analog plots shown in experimental animal studies (e.g., Ren and Nuttall, 2001; Rhode, 2007). The intermediate nonlinear transition between two asymptotic linear regimes is clearly visible. In a log-log plot, linear behavior corresponds to unitary slope, and the horizontal shift is a measure of the maximum active gain provided by the OHC mechanism.

For the above parameters of the AD model, the maximum active gain is expected to be 20 dB. The theoretical dependence of this gain on the ratio between the BM rms displacement and the saturation displacement has been already shown in Fig. 1. From the simulations of Fig. 3 one can compute the OHC active (amplitude) gain at different stimulus levels, and compare it to the theoretical expressions derived in the previous section. The maximum active gain is shown in the top panel of Fig. 7, as a function of the stimulus level. In this case the active gain is the ratio between the maximum amplitude of the resonant response and the stimulus level, expressed in a dB scale relative to the asymptotic constant value of this ratio reached at very high stimulus levels, for which the response returns that of the underlying

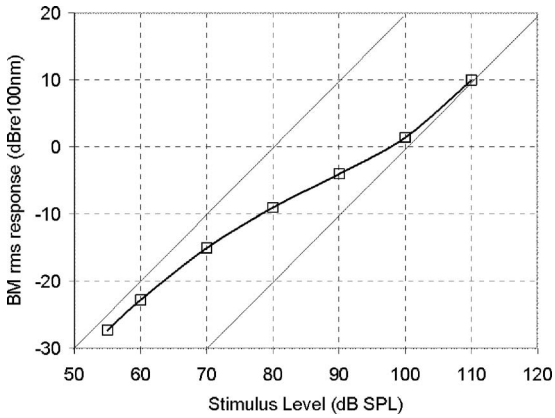


FIG. 6. Dependence on the stimulus level of the peak response of the AD model with Q=2 and $\alpha_0$=0.9, shown in Fig. 3. The intermediate nonlinear transition between two asymptotic linear regimes is visible, as in animal experiments. In a log-log plot, linear behavior corresponds to unitary slope, and the horizontal shift (in this case, slightly less than 20 dB) is a measure of the maximum active gain.

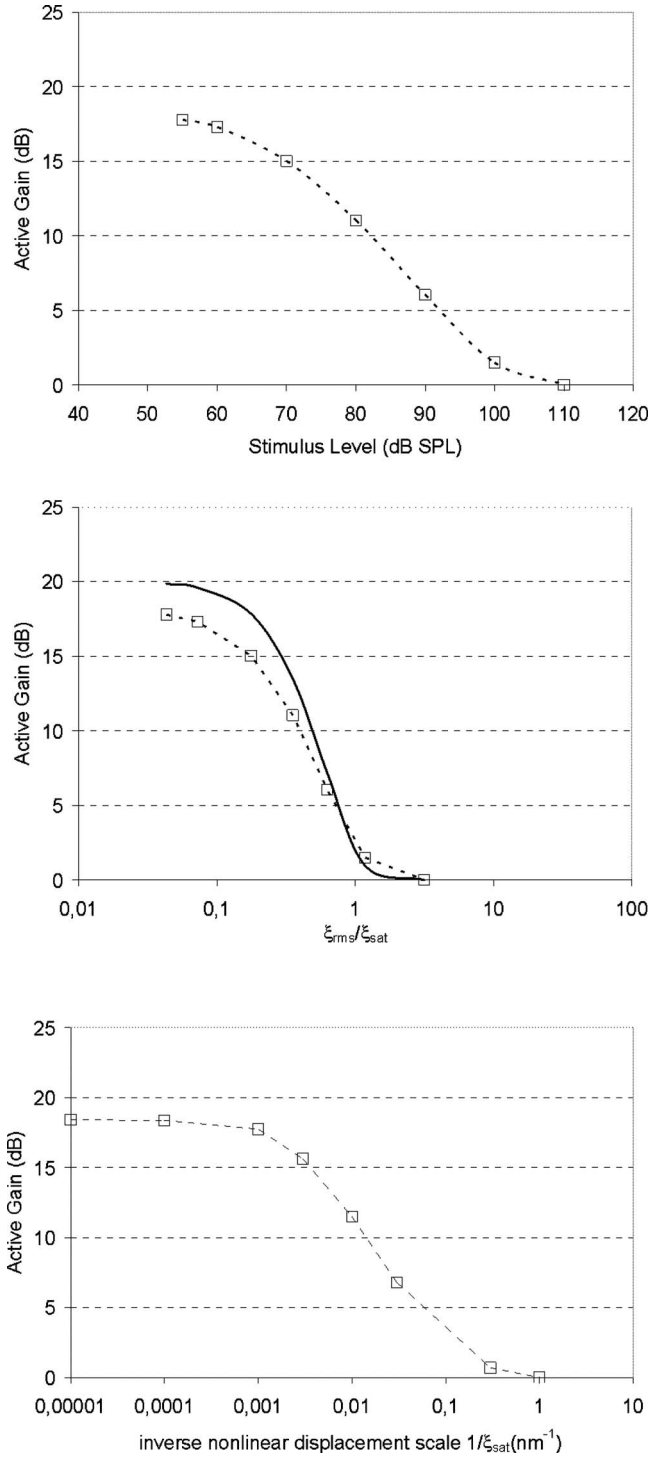


FIG. 7. (Top panel) Cochlear active gain derived from the data of Fig. 6, as a function of the stimulus level. The slow nonlinear decrease of the active gain is visible; (mid) same cochlear gain plotted against the ratio between the BM rms displacement and the saturation displacement, along with the theoretical gain of Fig. 1; (bottom) active gain dependence on the inverse of the nonlinear displacement scale, for a fixed stimulus level of 80 dB SPL.

passive linear model. The slow decrease of the active gain is observed to extend over a wide stimulus range, associated with a correspondingly nonlinear cochlear response. In the mid panel of Fig. 7 the same data are plotted against the ratio between the BM rms displacement and the saturation displacement, along with the correspondent theoretical gain of Fig. 1. The dependence of the gain on stimulus level is obviously slower than that on BM displacement, because, in the nonlinear range, BM displacement is a slowly varying function of the stimulus level itself. The comparison with the theoretical prediction shows a good agreement, although the expected maximum gain is not fully achieved, and that the dependence is slightly slower relative to the theoretical one, which, however, was a rough estimate valid for a point-like system only. The small difference may be attributable to the nonlocality of the active term and to the evolution of the solution amplitude during the forward TW propagation along the BM. The active gain dependence on the inverse of the nonlinear displacement scale is shown in the bottom panel of Fig. 7, for a fixed stimulus level of 80 dB SPL: the gain goes to unity (passive system limit) for low values of $\xi_{sat}$, and approaches the theoretical maximum gain for high values of $\xi_{sat}$. As expected, the gain dependence on this parameter mirrors that on the response level, because the gain regime is set in Eq. (33) by the ratio between the actual BM displacement $\xi$ and $\xi_{sat}$, which can be increased either by increasing the stimulus, and therefore the response, or by decreasing the saturation level at a fixed stimulus level.

In Fig. 8 we show the maximum active gain as a function of the stimulus level (top panel) and of the ratio between the maximum BM displacement and the nonlinear damping scale (mid panel), for the two considered FF models ($Q=2$, $\alpha_0=0.7$; $Q=8$, $\alpha_0=0.6$). In the bottom panel of Fig. 8 the active gain is shown as a function of the nonlinear displacement scale for the FF model with $Q=8$, $\alpha_0=0.6$. A first observation is that the maximum gain is higher for the higher passive $Q$ model, even for a smaller value of the gain parameter ($\alpha_0=0.6$, instead of 0.7). The response of the FF model appears to be less predictable than that of the AD model, requiring therefore accurate numerical simulations in different regions of its key parameters. The comparison with Fig. 7 shows that the dependence of the active gain on stimulus level and nonlinear displacement scale is quite similar for the AD and FF models, confirming that, as regards peak gain only, it is possible to find a FF model that is "equivalent" to a given AD model.

### C. Width of the activity patterns

As previously discussed, an active OHC term proportional to pressure is effective in a broader and more basal region than a classical AD force proportional to the BM velocity, which is maximum around the resonance place. As an important consequence, which perhaps has not been given the deserved consideration in the literature, the FF term proportional to pressure proposed by Lim and Steele (2002) also reproduces one of the key properties of the "Zweig" delayed-stiffness terms (Zweig, 1991), namely that the region of "effective negative damping," if present, is shifted toward the base with respect to the resonant place. As it is well known, this feature is desired to get the tall-and–broad activity patterns and the phase experimentally observed in classical studies of the BM vibration response to tones (Rhode, 1971).

This effect is visible in Fig. 9, where a comparison is shown between the BM displacement profiles (for each $x$, amplitude and phase of the $f_0$ component of the FT of the

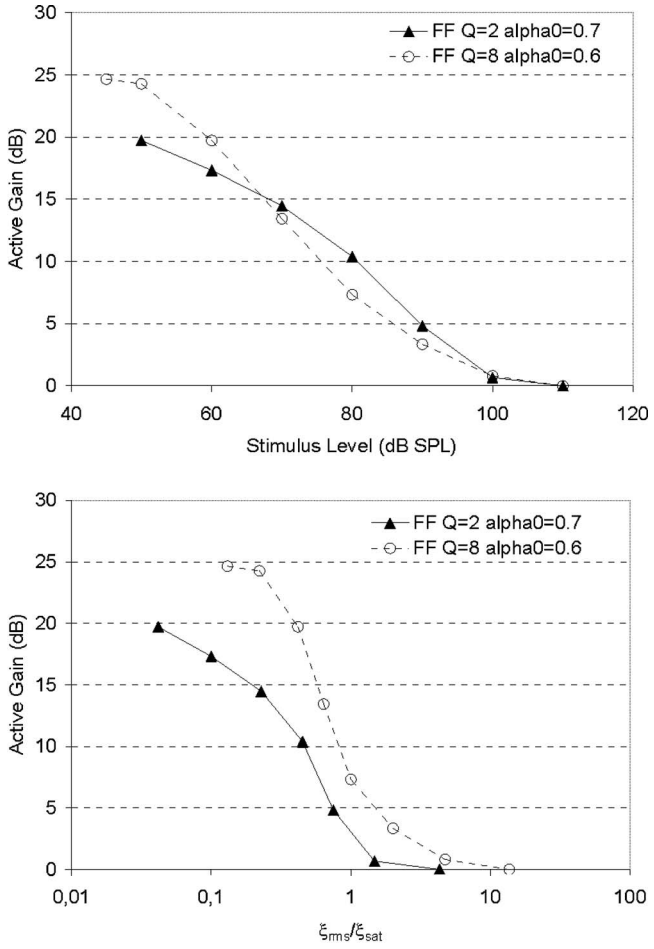


FIG. 8. (Top panel) Cochlear active gain for the two FF models of Figs. 4 and 5, plotted as a function of the stimulus level; (mid) same cochlear gain plotted against the ratio between the BM rms displacement and the saturation displacement; (bottom) active gain dependence on the inverse of the nonlinear displacement scale, for a fixed stimulus level of 80 dB SPL, for the FF model of Fig. 5.

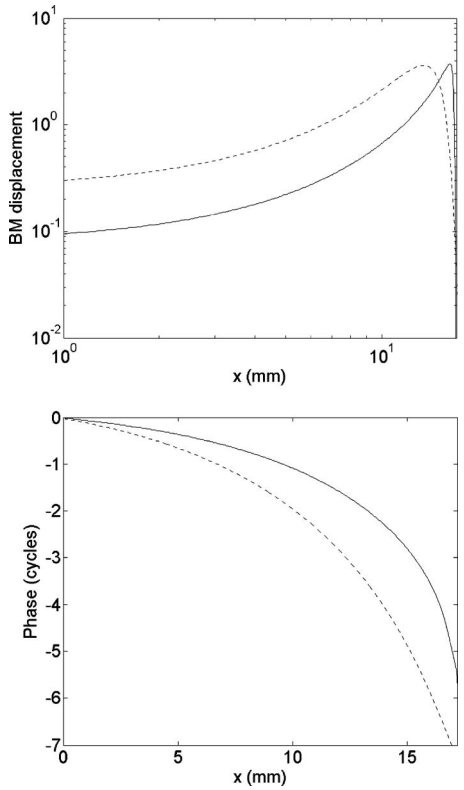


FIG. 9. BM displacement profiles for a diagonal model with additional AD force proportional to BM velocity (solid line), and for a feed-forward model with additional force proportional to total pressure (dotted line), with passive $Q=2$, $\alpha_0=0.9$ and 0.7, respectively, for a stimulus level of 60 dB SPL. The model with additional pressure produces a much broader response pattern at the same gain level.

local BM response) obtained (for a stimulus level of 60 dB SPL) for: (1) a diagonal model with additional force proportional to BM velocity (solid line), (2) a FF model with additional force proportional to total pressure (dotted line), both with passive $Q=2$ and, respectively, $\alpha_0=0.9$ and $\alpha_0=0.7$, which as discussed above, approximately correspond to the same maximum active gain. The comparison confirms that the model with additional force proportional to pressure produces, at the same BM response levels, a much broader response pattern.

### D. Phase slope and cochlear transmission delay

The decrease of the phase slope with increasing stimulus level that is visible in Figs. 3–5 can be converted, in a scale-invariant model, into an estimate of the dependence on stimulus level of the group delay, which provides a measure of the forward cochlear transmission latency:

$$\tau = -\frac{\partial \phi}{\partial \omega} = \frac{\partial \phi}{\partial x}\frac{\partial x}{\partial \omega} = -\frac{1}{\omega k_\omega}\frac{\partial \phi}{\partial x}. \tag{47}$$

The result is shown in Fig. 10 for the three models. Open symbols refer to the slopes computed at the actual peak position of each response, which shifts toward the base with increasing stimulus level. This estimate should be strictly related to the actual half-latency of the TEOAE response, because the generation of the reflected backward wave is generally assumed to occur near the peak of the response (Talmadge *et al.*, 2000), and to the forward cochlear transmission contribution to the ABR latency. The estimated value of the latency and its dependence on the stimulus level are quite variable among the three considered models, and strongly dependent on the choice of the position where the slope is measured. Within this huge uncertainty, the estimated latency decreases steadily with increasing stimulus level, in agreement with estimates of the forward latency

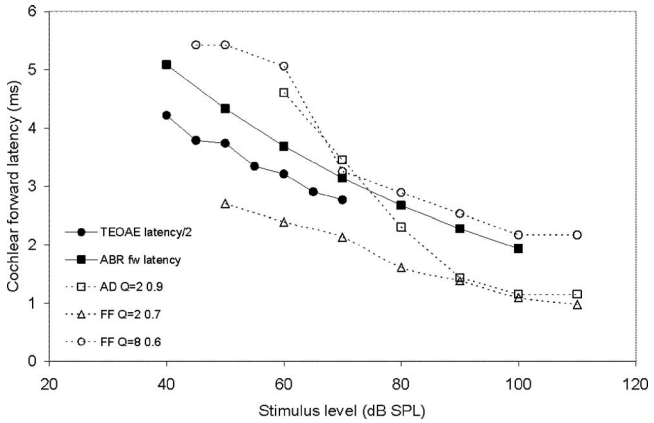


FIG. 10. Estimates of the forward TW transmission latency at 2 kHz obtained by measuring the slope of the phase/position relation shown in Figs. 3–5. Open symbols represent latencies derived from the slopes at the actual peak position of each response. Black symbols are used to show, for comparison, some ABR and TEOAE estimates of the forward cochlear latency (from Moleti and Sisto, 2008). TEOAE stimulus levels have been converted from dB pSPL to dB SPL by subtracting 20 dB, to approximately account for the click bandwidth.

derived from ABR and TEOAE latency experimental observations in humans [full symbols are ABR latency data derived from Neely *et al.* (1988) and TEOAE latency data from Sisto and Moleti (2007) as reported by Moleti and Sisto (2008)]. According to theoretical predictions, the transmission latency decreases with increasing stimulus level due to decreased tuning of the cochlear nonlinear active filter (Moleti and Sisto, 2003).

## IV. CONCLUSIONS

Time-domain numerical solutions of cochlear models with different nonlinear terms schematizing the OHC feedback demonstrate the capability of such models to capture some key features of the cochlear nonlinear mechanics, using a limited number of parameters. The state space formalism provides a very convenient framework for the implementation of such models. A discussion of how and why different modeling choices affect the measurable properties of the predicted BM response has been attempted, to get useful hints about how to design a model in agreement with experimental BM response, electrophysiological and otoacoustic data. The model has been also designed to describe otoacoustic emission generation, adding cochlear roughness as an additional parameter, to compare the model predictions with otoacoustic data. This issue will be the object of dedicated forthcoming studies.

## ACKNOWLEDGMENT

The contribution of D. Bertaccini has been partially supported by PRIN Grant 20083KLJEZ.

Bertaccini, D., and Fanelli, S. (**2009**). "Computational and conditioning issues of a discrete model for sensorineaural hypoacusia," Appl. Numer. Math. **59**, 1989–2001.
de Boer, E., and Nuttall, A. L. (**2009**). "Inverse-solution method for a class of non-classical cochlear models," J. Acoust. Soc. Am. **125**, 2146–2154.
de Boer, E., Zheng, J., Porsov, E., and Nuttall, A. L. (**2008**). "Inverted direction of wave propagation (IDWP) in the cochlea," J. Acoust. Soc. Am. **123**, 1513–1521.
Dong, W., and Olson, E. S. (**2008**). "Evidence for reverse cochlear traveling waves," J. Acoust. Soc. Am. **123**, 222–240.
Elliott, S. J., Ku, E. M., and Lineton, B. (**2007**). "A state space model for cochlear mechanics," J. Acoust. Soc. Am. **122**, 2759–2771.
Furst, M., and Lapid, M. (**1988**). "A cochlear model for acoustic emissions," J. Acoust. Soc. Am. **84**, 222–229.
Geisler, C. D., and Sang, C. (**1995**). "A cochlear model using feed-forward outer-hair-cell forces," Hear. Res. **86**, 132–146.
Greenwood, D. D. (**1990**). "A cochlear frequency position function for several species—29 years later," J. Acoust. Soc. Am. **87**, 2592–2605.
He, W., Nuttall, A. L., and Ren, T. (**2007**). "Two-tone distortion at different longitudinal locations on the basilar membrane," Hear. Res. **228**, 112–122.
Kanis, L. J., and de Boer, E. (**1993**). "Self-suppression in a locally active nonlinear model of the cochlea: A quasilinear approach," J. Acoust. Soc. Am. **94**, 3199–3206.
Kim, J., and Xin, J. (**2005**). "A two-dimensional nonlinear nonlocal feed-forward cochlear model and time domain computation of multitone interactions," Multiscale Model. Simul. **4**, 664–690.
Ku, E. M. (**2008**). "Modelling the human cochlea," Ph.D. thesis, University of Southampton, United Kingdom.
Lim, K. M., and Steele, C. R. (**2002**). "A three-dimensional nonlinear active cochlear model analyzed by the WKB-numeric method," Hear. Res. **170**, 190–205.
Moleti, A., Paternoster, N., Bertaccini, D., Sisto, R., and Sanjust, F. (**2009**). "Otoacoustic emissions in time-domain solutions of nonlinear non-local cochlear models," J. Acoust. Soc. Am. **126**, 2425–2436.
Moleti, A., and Sisto, R. (**2003**). "Objective estimates of cochlear tuning by otoacoustic emission analysis," J. Acoust. Soc. Am. **113**, 423–429.
Moleti, A., and Sisto, R. (**2008**). "Comparison between otoacoustic and auditory brainstem response latencies supports slow backward propagation of otoacoustic emissions," J. Acoust. Soc. Am. **123**, 1495–1503.
Neely, S. T., and Kim, D. O. (**1986**). "A model for active elements in cochlear biomechanics," J. Acoust. Soc. Am. **79**, 1472–1480.
Neely, S. T., Norton, S. J., Gorga, M. P., and Jesteadt, W. (**1988**). "Latency of auditory brain-stem responses and otoacoustic emissions using tone-burst stimuli," J. Acoust. Soc. Am. **83**, 652–656.
Nobili, R., and Mammano, F. (**1996**). "Biophysics of the cochlea II: Stationary nonlinear phenomenology," J. Acoust. Soc. Am. **99**, 2244–2255.
Puria, S. (**2003**). "Measurements of human middle ear forward and reverse acoustics: Implications for otoacoustic emissions," J. Acoust. Soc. Am. **113**, 2773–2789.
Ren, T., and Nuttall, A. L. (**2001**). "Basilar membrane vibration in the basal turn of the sensitive gerbil cochlea," Hear. Res. **151**, 48–60.
Rhode, W. S. (**1971**). "Observations of the vibration of the basilar membrane in squirrel monkeys using the Mössbauer technique," J. Acoust. Soc. Am. **49**, 1218–1231.
Rhode, W. S. (**2007**). "Basilar membrane mechanics in the 6–9 kHz region of sensitive chinchilla cochleae," J. Acoust. Soc. Am. **121**, 2792–2804.
Shera, C. A. (**2003**). "Mammalian spontaneous otoacoustic emissions are amplitude-stabilized cochlear standing waves," J. Acoust. Soc. Am. **114**, 244–262.
Shera, C. A., Tubis, A., and Talmadge, C. L. (**2005**). "Coherent reflection in a two-dimensional cochlea: Short-wave versus long-wave scattering in the generation of reflection-source otoacoustic emissions," J. Acoust. Soc. Am. **118**, 287–313.
Shera, C. A., Tubis, A., Talmadge, C. L., de Boer, E., Fahey, P. F., and Guinan, J. J., Jr. (**2007**). "Allen–Fahey and related experiments support the predominance of cochlear slow-wave otoacoustic emissions," J. Acoust. Soc. Am. **121**, 1564–1575.
Sisto, R., and Moleti, A. (**2007**). "Transient evoked otoacoustic emission latency and cochlear tuning at different stimulus levels," J. Acoust. Soc. Am. **122**, 2183–2190.
Talmadge, C. L., Tubis, A., Long, G. R., and Piskorski, P. (**1998**). "Modeling otoacoustic emission and hearing threshold fine structures," J. Acoust. Soc. Am. **104**, 1517–1543.
Talmadge, C. L., Tubis, A., Long, G. R., and Tong, C. (**2000**). "Modeling the combined effects of basilar membrane nonlinearity and roughness on stimulus frequency otoacoustic emission fine structure," J. Acoust. Soc. Am. **108**, 2911–2932.
Voss, S. E., and Shera, C. A. (**2004**). "Simultaneous measurement of middle-ear input impedance and forward/reverse transmission in cat," J. Acoust. Soc. Am. **116**, 2187–2198.
Zweig, G. (**1991**). "Finding the impedance of the organ of Corti," J. Acoust. Soc. Am. **89**, 1229–1254.